High-current stream of energetic α particles from laser-driven proton-boron fusion

Lorenzo Giuffrida,[1,*] Fabio Belloni,[2] Daniele Margarone,[1] Giada Petringa,[3] Giuliana Milluzzo,[3,†] Valentina Scuderi,[1,3] Andriy Velyhan [ORCID],[1] Marcin Rosinski,[4] Antonino Picciotto [ORCID],[5] Milan Kucharik [ORCID],[6] Jan Dostal,[7,8] Roman Dudzak,[7,8] Josef Krasa [ORCID],[8] Valeria Istokskaia [ORCID],[1,6] Roberto Catalano,[3] Salvatore Tudisco,[3] Claudio Verona,[9] Karel Jungwirth,[8] Pierluigi Bellutti,[5] Georg Korn,[1] and G. A. P. Cirrone[1,3]

[1]*Institute of Physics ASCR, v.v.i (FZU), ELI-Beamlines, 182 21, Prague, Czech Republic*
[2]*European Commission, Directorate-General for Research and Innovation, Euratom Research, Brussels, Belgium*
[3]*Laboratori Nazionali del Sud, INFN, Catania, Italy*
[4]*Institute of Plasma Physics and Laser Microfusion, 01-497 Warsaw, Poland*
[5]*Micro-Nano Facility, Center for Materials and Microsystems, Fondazione Bruno Kessler, Trento, Italy*
[6]*Czech Technical University in Prague, Faculty of Nuclear Sciences and Physical Engineering, 115 19 Prague, Czech Republic*
[7]*Institute of Plasma Physics of the Czech Academy of Sciences, Prague 8, 182 00 Czech Republic*
[8]*Institute of Physics of the Czech Academy of Sciences, Prague 8, 182 21 Czech Republic*
[9]*INFN–Dipartimento di Ingegneria Industriale, Università di Roma 'Tor Vergata,' Rome, Italy*

The nuclear reaction known as proton-boron fusion has been triggered by a subnanosecond laser system focused onto a thick boron nitride target at modest laser intensity ($\sim 10^{16}$ W/cm^2), resulting in a record yield of generated α particles. The estimated value of α particles emitted per laser pulse is around 10^{11}, thus orders of magnitude higher than any other experimental result previously reported. The accelerated α-particle stream shows unique features in terms of kinetic energy (up to 10 MeV), pulse duration (~ 10 ns), and peak current (~ 2 A) at 1 m from the source, promising potential applications of such neutronless nuclear fusion reactions. We have used a beam-driven fusion scheme to explain the total number of α particles generated in the nuclear reaction. In this model, protons accelerated inside the plasma, moving forward into the bulk of the target, can interact with ^{11}B atoms, thus efficiently triggering fusion reactions. An overview of literature results obtained with different laser parameters, experimental setups, and target compositions is reported and discussed.

I. INTRODUCTION

The interaction of protons with ^{11}B atoms can trigger a neutronless nuclear reaction known as proton-boron (pB) fusion,

$$^{11}\text{B} + \text{p} \rightarrow 3\alpha + 8.7\,\text{MeV}, \qquad (1)$$

discovered in the 1930s by Oliphant and Rutherford [1]. In such reaction, predominant at energies below 10 MeV [2–7], the final product is the generation of three energetic α particles. Several theoretical and experimental studies report a main resonance peak occurring at 675 keV proton energy in the lab, with a maximum cross section of 1.2 barn [8,9] [Fig. 1(a)]. A second resonance at 160 keV has a maximum cross section of about 100 mbarn. The generated α particles have a large energy spectrum strongly peaked around 4 MeV. In a simplified view, on average one α particle is emitted with an energy of 1 MeV and the other two with the energy of 4 MeV [4].

In the last decades, the interest of the scientific community in the pB fusion reaction has grown because of its potential applications in different fields. For example, different papers have focused on the neutronless production of energetic α particles, which may allow building an "ultraclean" fusion reactor [10–13], despite the low reactivity of H^{11}B fuel compared to conventional DT fuel [Fig. 1(b)]. α particles generated by the ^{11}B (p,α)2α reaction could also be used for neutronless nuclear-fusion-based-propulsion in space [14].

Recently, much interest has focused on using the α particles generated by such reaction for cancer treatments in human bodies. According to Yoon *et al.* [15] and Giuffrida *et al.* [16], based on Monte Carlo simulations, cancer treatment using the pB reaction could produce an enhancement of the treatment biological effectiveness, if compared with standard proton therapy. Experimental campaigns conducted in-vivo on boron-treated cancer cells by Cirrone *et al.* [17] demonstrated the potential clinical efficacy of this approach. Moreover, Petringa *et al.* [18,19] proposed that prompt γ's emitted in the pB reactions could be used for on-line proton beam imaging purposes during cancer treatment, also reported in Refs. [15,16].

In 2005 Belyaev *et al.* [20] experimentally demonstrated, for the first time, the possibility to trigger the pB fusion reaction by using an intense ps laser beam (2×10^{18} W/cm^2) interacting with a boron-rich polymeric target. In this

---
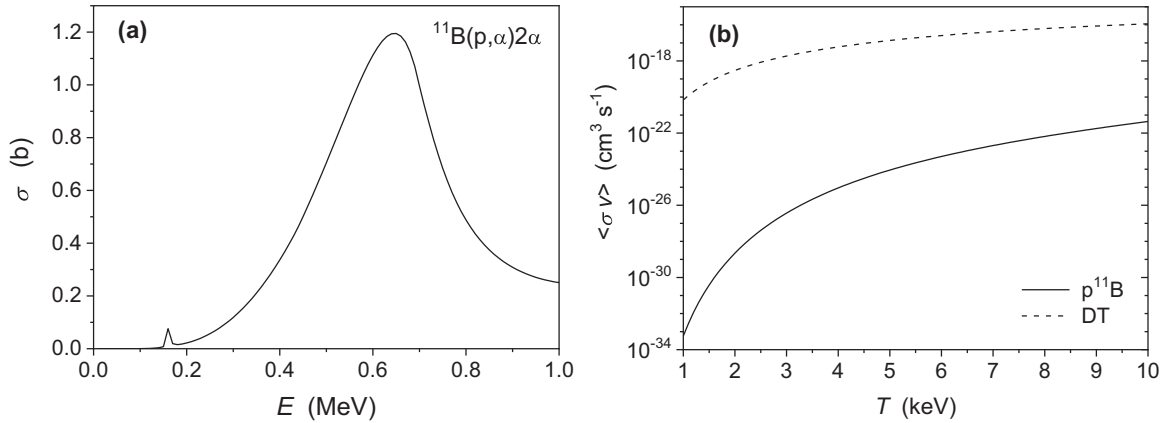
FIG. 1. (a) p-^{11}B fusion cross section as a function of proton energy in the lab, based on the analytic approximation of Nevins and Swain [2]. (b) Low-temperature reactivity for pB fusion and, as a term of comparison, DT fusion. Plots are based on the analytic approximations of Refs. [2] and [25], respectively.

experiment, protons generated by laser-target interaction and hitting B atoms in the bulk of the target can induce the nuclear reaction. An α-particle yield of about 10^3 α/sr/shot was estimated in this experiment, later corrected by Kimura *et al.* [21] to a final yield of 10^5 α/sr/shot.

In 2013 Labaune *et al.* [22] published results of an experiment performed using the LULI laser system in France. In this experiment they used two laser beams: the first, having ns pulse duration, to ionize a solid B target, the second, having shorter duration (ps regime) but very high intensity (6×10^{18} W/cm^2), to accelerate the proton beam via a second target. They demonstrated a maximum α-particle yield of about 9×10^6 α/sr/shot, much higher than previously reported. Almost simultaneously, Picciotto *et al.* [23], with a setup similar to that of Ref. [20] but using a sub-ns laser with modest intensity (10^{16} W/cm^2) at the Prague Asterix Laser System (PALS) in the Czech Republic, obtained a much higher number of α particles (around 10^9 α/sr/shot). In particular, they used a hydrogenated silicon target, doped by boron through ion implantation and enriched with hydrogen by an annealing process. A second experimental campaign [24] confirmed those results, using different types of target and different thicknesses.

In this paper, we report an even higher yield of α particles, well above 10^{10} α/sr/shot, obtained on boron nitride (BN) thick target at PALS. We also report a spectral and angular characterization of the α particles emitted. In particular, we find the first evidence of laser-induced acceleration in the α spectrum. Finally, we propose an original explanation for the mechanism of α production and transport.

Our findings are very promising in view of a possible feasibility proof of laser-driven pB fusion as an energy source. As a matter of fact, hydrodynamic simulations by Hora *et al.* [12,13] show that the ignition of a fusion flame is possible in solid-density H^{11}B fuel under irradiation with a high-contrast laser pulse in the ps-PW regime and the effect of magnetic confinement at field strengths of the order of 10 kTesla.

II. EXPERIMENTAL SETUP

The experimental campaign was performed at the PALS laser facility in Prague (Czech Republic) using an iodine laser working at the fundamental wavelength of 1315 nm, 600 J pulse energy, and sub-ns duration (0.3 ns FWHM) [25]. The laser beam was focused onto the target inside a vacuum chamber (with a pressure lower than 10^{-5} mbar) with an incidence angle of 30° with respect to the target normal and a spot diameter of about 80 μm allowing one to reach an optimal intensity on target of about 3×10^{16} W/cm^2.

Half-mm-thick BN targets were irradiated to trigger the pB fusion reaction. The target density was $\rho_0 = 2.1$ g/cm^3. Natural boron is composed of two stable isotopes, ^{10}B and ^{11}B, in the ratio ^{11}B/^{10}B = 4. Boron nitride is obtained by reacting trioxide (B$_2$O$_3$) or boric acid (H$_3$BO$_3$) with ammonia (NH$_3$) or urea (CO(NH$_2$)$_2$) in a nitrogen atmosphere [26]. The content of hydrogen, as a source of protons, is directly related to the chemical synthesis of the material. The BN targets were provided by the Micro-Nano Facility of the Fondazione Bruno Kessler.

Since the thickness of the target does not allow the generated particles (laser-accelerated ions and α particles from the pB reaction) to penetrate through it, detectors were placed only in the backward direction (with respect to the laser propagation). Due to the target thickness, it is impossible to retrieve any useful information about the stream of particles in the forward direction (target rear side) as is possible in the case of fusing deuterons [27]. A sketch of the experimental setup is depicted in Fig. 2.

Several solid state silicon carbide (SiC) detectors [28,29], working in a time-of-flight (TOF) configuration [29–31], were placed at different angles with respect to the target normal (on the same plane, from −21° to +66°, entailing different distances from the target). These detectors were used to measure, shot-to-shot, the energy distribution and the flux of the charged particles (protons and α particles) emitted from the target. By doing so, it was possible to map the angular distribution in the *back* hemisphere. Thin Al foils of different thickness (from few to 15 μm) have been placed in front of the TOF detectors to stop the slower ion components and disentangle protons and α particles reaching the detectors at the same TOF values.

Several CR39 nuclear track detectors [32], previously calibrated using an ^{241}Am source, were placed at the same
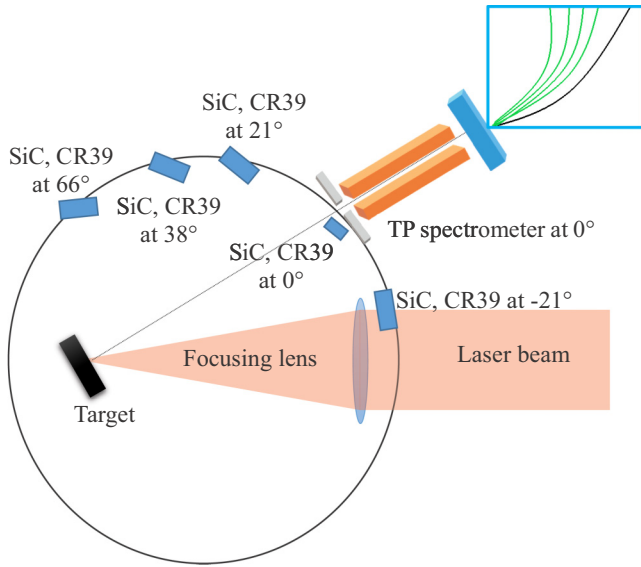
FIG. 2. Experimental setup used during this experimental campaign. The laser beam passing through a focusing lens reaches a final dimension of 80 μm onto the target (30° incidence angle). Particle emission is mainly along the normal to the target surface. Several detectors (SiC and CR39) were placed at different angles. A Thomson Parabola spectrometer (TP) was placed at 0°.

angles of the SiC detectors. CR39 detectors were allowed to measure the absolute number of α particles and protons. A mask, having four Al filters of different thickness (from 6 to 15 μm), was placed in front of each CR39 in order to filter the low-energy ion component out, since it was not relevant for the goal of the experiment, and to avoid overlap of neighboring ion tracks. The filtering technique is also useful for studying the energy distribution of α particles reaching the nuclear track detector.

A Thomson Parabola (TP) spectrometer, equipped with a microchannel plate detector, was placed along the target normal to distinguish different ion species in the plasma plume and estimate the proton energy cutoff and distribution. For cross-checking results from the TP, a SiC detector and a set of nuclear track detectors were installed very close to the TP entrance slit.

III. EXPERIMENTAL RESULTS

Figure 3(a) reports TOF signals acquired with two 27 μm SiC detectors placed at two different angles: along the target normal (black curve) and at 66° (red curve).

Signals are normalized at 1 m distance to be comparable as reported in Ref. [33]. The signal recorded from the detector at 0° is a typical TOF spectrum from laser-driven ion acceleration, containing different ion components from the plasma emission: protons, B, N, and C ions (from surface contaminants). This is mixed with the signal (peaks) coming from the α-particle component, which is generated by the pB reaction. However, the signal recorded by the detector at 66° shows a rather different behavior. There are two intense and distinct peaks at about 50 ns and 70 ns, respectively, which are absent at smaller angles and are not ascribed to

plasma ions. In fact, it is known that, in this laser intensity regime, the emission of laser-driven ions is mainly contained inside a cone not larger than 30°–40° [34]. Consequently, the plasma ion signal recorded at large angles is expected to be drastically reduced if compared with the signal recorded at small angles. On the contrary, the α particle emission from the nuclear fusion reaction, independently from the angular distribution of plasma ions, is expected to reach the detector even at large angles. Finally, the signal recorded at 66° cannot be ascribed to plasma ions because its intensity is very strong and comparable with the intensity of plasma ions at 0° (preferential acceleration direction), although the ion detectors are equipped with Al filters to stop slower ions.

For a better understanding of the incoming ion signal, a comparison with results from the TP spectrometer is needed. Figure 3(b) shows raw data recorded by the TP (at 0°) in the same shot of Fig. 3(a). The signal is composed of several parabolas corresponding to different ion species. The proton parabola, the lowest and less intense one, is of interest in this analysis. The corresponding energy distribution is reported in Fig. 3(c). The measured maximum proton energy is 1.5 MeV. This energy value was used as a starting point for interpreting the TOF spectra.

The beginning of the signal recorded by TOF detectors at 0° and 66°, corresponding to about 45 ns and representing the fastest ion component, is incompatible with the maximum proton energy measured with the TP or with any other ion signal from the plasma (N, B, or other contaminants). Indeed, protons recorded with this TOF should have an energy around 2.5 MeV. We believe that the first peak clearly measured by the detector placed at 66° is mainly due to α particles with energies between 5 and 10 MeV, and the second peak can be ascribed to α particles between 3 and 5 MeV. The weak signal in between these peaks is due to the small number of protons and other light ions at this large angle.

The final determination of the α energy spectra, using the technique described in Ref. [30], is presented in Fig. 3(d). Despite the fact that the pB fusion reaction at the 675 keV resonance takes place in the s wave [4], slight anisotropy is expected in the lab, in both α-particle yield and energy distribution, owing to the initial proton momentum, when ^{11}B is at rest [Fig. 3(e)]. The comparison between the experimental spectra at 0° and 66° actually shows a strong anisotropy. Another important remark comes from the maximal spectral energy reaching 10 MeV, a value much higher than the expected endpoint. It is easy to calculate that for an incoming proton of 675 keV, the spectral endpoint of the produced α particles is located at about 6.7 MeV in the lab (α_0 channel [6]). At the highest proton energies recorded in our experiment, around 1.5 MeV, the endpoint is expected to reach 7.3 MeV. Moreover, we observe also that the two maxima in the theoretical spectra (at about 1 and 4 MeV, respectively) are rightward-shifted by 3–4 MeV, depending on the detection angle. We believe that the energy shift as well as the marked anisotropy in the measured spectra is due to the action of the same electric field, generated in the proximity of the critical-density surface, which accelerates plasma ions in the backward direction [35]. This field, which is moreover far from being uniform, is generated by
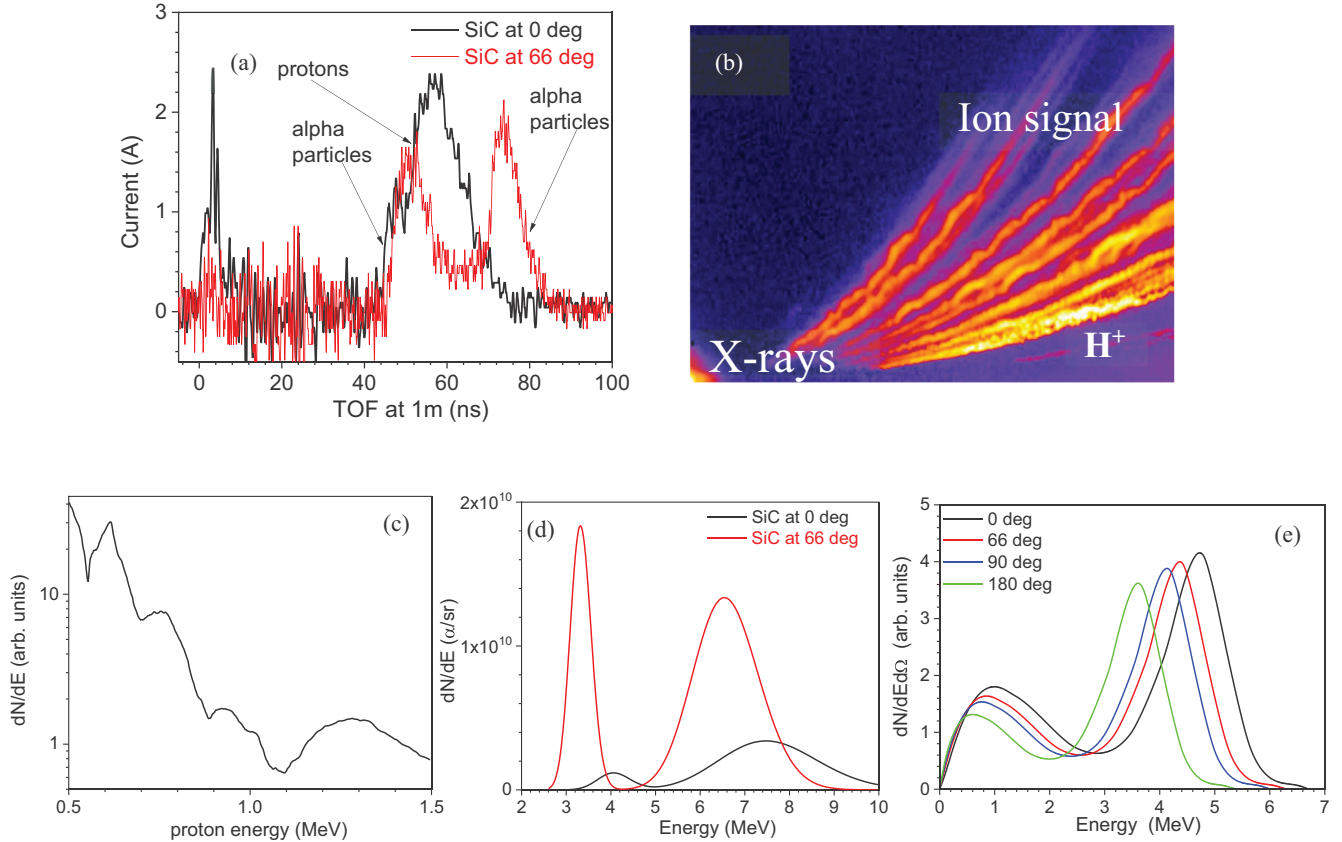
FIG. 3. (a) TOF spectra from detectors placed at 0° (black curve) and 66° (red curve) normalized at 1 m distance. (b) Raw data from TP spectrometer, showing the different ion species deflected from the electric and magnetic field of the detector. (c) Proton energy distribution from the TP evaluation. The measured data have been smoothed, in the black line, to better understand the behavior of the distribution. (d) α-particle energy distribution from TOF deconvolutions at 0° (black curve) and 66° (red curve). (e) Theoretical spectra in the reaction channel via $^8\text{Be}^*$, for different values of the detection angle θ. Calculations refer to a 675 keV proton impinging on ^{11}B at rest along $\theta = 0$ (after Stave *et al.* [4]).

differences of quasi-electrostatic potential that may indeed be as high as 1.5 MV, according to the maximum proton energy we measure. To summarize, the measured energy of 10 MeV for α particles is given by the endpoint of 7.3 MeV summed to $2 \times (1.5 \text{ MeV})$.

Figure 4 reports an example of images obtained after 1 h etching of a set of nuclear track detectors placed at 66°, covered with Al filters of different thickness, respectively, 6 μm [Fig. 4(a)], 10 μm [Fig. 4(b)], 12 μm [Fig. 4(c)], and 15 μm [Fig. 4(d)]. The black dots represent α particles, while the lightest and smallest dots represent the proton signal. The thinnest Al filter can cut only ions and α particles with relatively low energies, so that the flux on the detector is very high. As can be seen in Fig. 4(a), the signal is completely saturated; the 6 μm filter transmits protons and α particles with energies above 500 keV and 2 MeV, respectively. The increase of the filter thickness reduces the number of particles able to reach the detector, giving the possibility to have distinguishable tracks. In the case of a 15 μm filter, according to the calibration curve [Fig. 4(e)] and energy loss calculations [36], tracks with areas between 11 and 8 μm^2 are compatible with α particles having energies in the range 4.9–6.2 MeV. The smallest dark tracks, measuring less than 7 μm^2, are compatible with α particles with energies higher

than 7 MeV. This is in good agreement with results from the TOF deconvolutions shown in Fig. 3(d).

The integration of α-particle energy distributions from TOF spectra allowed us to estimate the α-particle yield per steradian at different angles, as reported in Fig. 5 (black dots). Because of the above mentioned 3–4 MeV shift in the energy distributions, the filter before the SiC detectors, with a 2 MeV cutoff, is supposed to leave the yield practically unaffected. The angular distribution obtained in this way has an increasing trend, with a minimum at 0° and a maximum measured value at 66°. The maximum measured yield is 2.8×10^{10} α/sr, a value much larger than any other estimation ever reported in previous experiments [20,22–24].

Because of some setup limitation in this experiment, it was not possible to explore angles larger than 66°. The peculiar shape of the angular distribution might be determined by the effect of the accelerating electric field—particularly, its spatial distribution—and by the attenuation or scattering of the α particles by the plasma plume. These effects are expected to contribute to the observed depletion of the α yield at small angles. We also put forward that, from basic kinematics, the propagation of isotropically emitted particles under the action of a longitudinal electric field may lead to the appearance of a limiting angle.
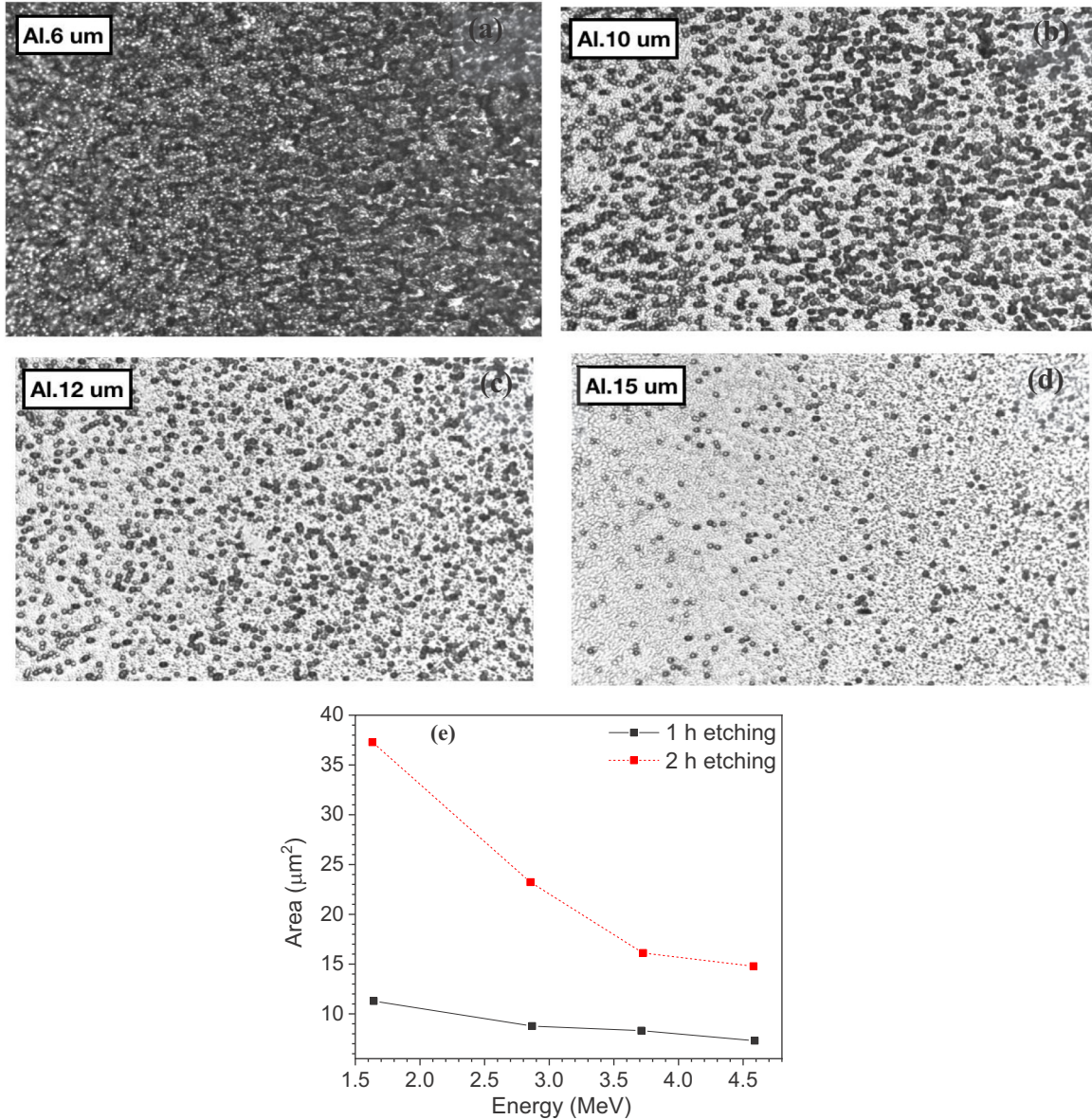
FIG. 4. Images from CR39 nuclear track detectors placed at 66°, covered with 6 μm (a), 10 μm (b), 12 μm (c), and 15 μm (d) Al filter, obtained after 1 h of etching time. (e) Evolution of the α-particles tracks as a function of the incident energy. The exposed CR39 were etched in a 6.05N NaOH solution at a constant temperature of 80°C. Different curves in the plot represent two different etching times: 1 h (black curve) and 2 h (red curve).

Results coming from the nuclear track detectors (red dots in Fig. 5) are in good agreement with TOF data points. The difference is mainly due to the different energy cutoff of the filters placed in front of the two detectors. Unfortunately, results from CR39 detectors at small angles cannot be reported because of the huge number of protons reaching the detectors that saturated even the detector area covered by the thickest filters.

The angular distribution is an important tool for estimating the total number of α particles produced by the pB reaction. Assuming symmetry around the target normal (comparing points at −20° and +21° in Fig. 5), the number of α particles emitted backward, $N_{\alpha,\text{back}}$, has been estimated by integrating the distribution from TOF measurements over the solid angle, for $\theta < 66°$, after fitting with a quadratic function. We

estimate $N_{\alpha,\text{back}} \simeq 6.5 \times 10^{10}$, which is a conservative value because of the constraint in the range of θ and likely flux attenuation at small angles. It is worth noticing, however, that the possible occurrence of a limiting angle beyond 66° would greatly mitigate the magnitude of the unaccounted large-angle contribution. Finally, we account for the number of the undetected α particles emitted in the forward direction by assuming isotropic emission, so that the total number of particles, $N_{\alpha,\text{tot}}$, is given by the obvious relationship

$$N_{\alpha,\text{tot}} \approx 2N_{\alpha,\text{back}} = 1.3 \times 10^{11}. \qquad (2)$$

Laser characteristics (intensity and spot size on target) and experimental setup (type of diagnostics) in this work are similar to those used by Picciotto *et al.* [23]; nevertheless
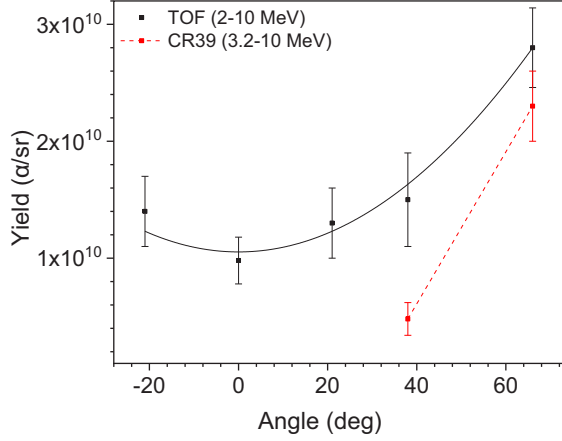
FIG. 5. Angular distribution obtained from TOF measurements (in black) compared with results obtained from CR39 (in red).

the total number of measured α particles in the backward direction is more than 150 times bigger. This is mainly due to the different target composition in terms of total number of available ^{11}B ions, not limited to a narrow implanted region (100 nm) as in Ref. [23]. In our case, indeed, the concentration of boron is 50% over the entire target.

IV. DISCUSSION

A. Modeling α-particle production

Thermonuclear yield: Initially, we have tried to explain the α yield in terms of thermonuclear reactions occurring in the plasma plume and the warm, shocked target bulk [37]. In the following, we denote by $\eta = \rho/\rho_0$ the compression ratio between the density under shock, ρ, and the initial (ordinary) bulk density, ρ_0. We briefly recall that compression ratios higher than the ideal-gas asymptotic value $\eta = 4$ can be achieved in single shocks induced by high-power laser pulses, with $\eta = 7$ being the upper bound for the maximum compression [38]. Simulations by means of a two-dimensional

hydrodynamic code employing the axisymmetric r-z geometry, Prague Arbitrary Lagrangian-Eulerian (PALE) [39], show the development of the compressed region in our case, during the onset of the laser pulse (Fig. 6). The compressed region reaches a width of about 3 μm and $\eta \simeq 6$ when laser intensity and delivered energy approach 10^{16} W/cm^2 and 50 J, respectively [at about 1.8 ns from the start of the laser-target interaction; Fig. 6(a)]. Beyond this *prepulse* regime (the FWHM portion of the pulse comes just afterwards), the reliability of the simulation is limited by factors such as the strong computational mesh degeneracy, especially at the highly deformed domain boundary, as well as the strong coupling between the plasma and bulk phases (including the effects of hot electrons).

Denoting by $N_{\alpha,th}$ the number of α particles produced via thermonuclear reactions in the interaction volume V during the confinement time τ, $N_{\alpha,th}$ is given by the usual relation

$$N_{\alpha,th} = 3\, n_p n_B \, \langle \sigma v \rangle V \tau, \tag{3}$$

where n_p and n_B are the number densities of protons and ^{11}B nuclei, respectively, $\langle \sigma v \rangle$ is the reactivity [Fig. 1(b)], and the factor of 3 is the number of α particles per reaction. Equation (3) holds for a well-defined interaction volume and constant, uniform densities of the reactants; on the other hand, these quantities rapidly vary in space and time across the plasma plume and shocked target. Moreover, the local density and temperature of plasma and target are poorly known in our experiment, as mentioned. Nevertheless, one can still reason about average, global quantities and try to estimate the product $n_B V$, i.e., the overall number of reacting ^{11}B nuclei, in terms of the plasma temperature T, which is easier to deal with. To this purpose, one can use the equation for the internal energy of an ideal gas, following isochoric heating by the laser pulse. If the gas is made of $(5/4)n_B$ boron nuclei per unit volume (the 5/4 factor accounts for the co-occurrent presence of the ^{10}B isotope), n_N nitrogen nuclei per unit volume, and $(5/4)n_B Z_B + n_N Z_N$ electrons per unit volume, one obtains

$$\frac{5}{4}(Z_B + Z_N + 2)n_B V \times \frac{3}{2}kT = E_L, \tag{4}$$
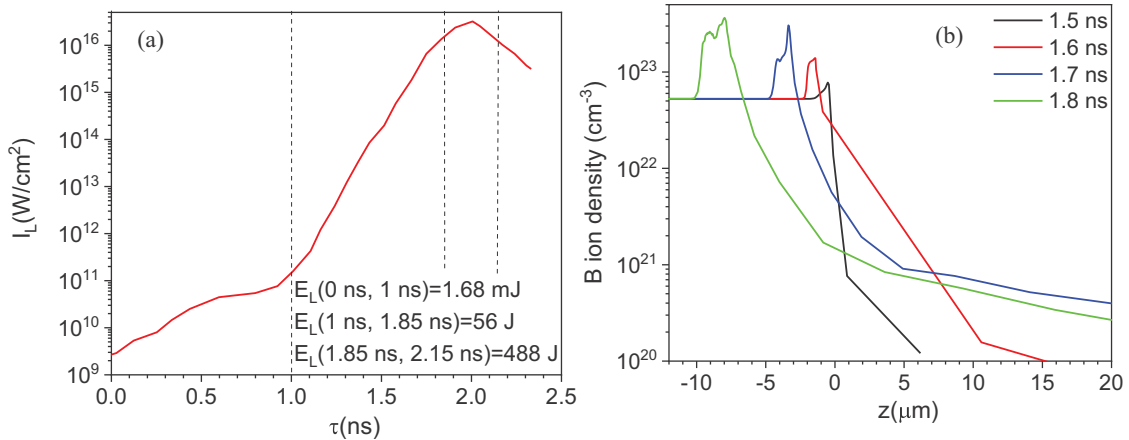
FIG. 6. (a) Temporal profile of the laser intensity on the target (measured). The laser energy contained in the time window up to 1.85 ns represents the prepulse of the laser. (b) PALE hydrodynamic simulation of the B ion density profile at different times from the start of the laser action ($t = 0$). Profiles are taken at the origin of the transverse coordinate (center of the laser spot). At $t = 0$, the longitudinal coordinate, z, is defined as follows: $z = 0$ is the target surface, $z > 0$ is a vacuum, and $z < 0$ is the target bulk.

where E_L is the laser energy, we have used the fact that $n_N = (5/4)n_B$ in BN, and we have neglected the contribution of H atoms (we recall that hydrogen comes as a contaminant in the BN target, i.e., $n_p \ll n_B$). We have also made the conservative assumption that the entire laser energy is absorbed by the medium and have neglected the internal degrees of freedom of the medium. With $n_B V$ given by Eq. (4), and $Z_B = 5$, $Z_N = 7$, Eq. (3) can now be recast in the form

$$N_{\alpha,th} = (4/35)n_p \tau E_L \langle \sigma v \rangle / kT. \tag{5}$$

As an estimate of the plasma temperature in our experiment, we have used the analytical model for plume expansion of Gus'kov *et al.* [37] and found a value of the order of 1 keV, which is in good agreement with, e.g., the temperature of C ions (1.8 keV) measured under similar irradiation conditions [40]. At $kT = 1$ keV, one finds $N_{\alpha,th} \simeq 3 \times 10^{-25} n_p$ (cm^{-3}) for $E_L = 600$ J and $\tau \sim 1$ ns. Getting to $N_{\alpha,th} = N_{\alpha,\text{tot}} \sim 10^{11}$ would require $n_p \sim 10^{36}$ cm^{-3}, which is absolutely unrealistic. Even pushing kT up to 10 keV would require, *ceteris paribus*, a yet unrealistic value for n_p of the order of 10^{25} cm^{-3}. On this basis, we are able to conclude that any thermonuclear contribution to the fusion yield is absolutely negligible in our experiment.

Finally, we have checked that even at the *suprasolidus* densities of the compressed target bulk, screening effects induced on the fusion reaction by electrons and ion correlation are still negligible. Indeed, for temperatures of the order of 1 keV or higher, we find a plasma parameter $\Gamma_{e(i)} = Z_B e^2 a_{e(i)} kT$ [41], which is much smaller than unity at both the average interelectron distance a_e and interion distance a_i, i.e., weakly coupled plasma. At lower temperatures, upon the assumption of complete ionization induced by pressure, the plasma becomes strongly coupled ($\Gamma_e, \Gamma_i > 1$). As an example, we find $\Gamma_e \simeq 10$ and $\Gamma_i \simeq 5$ at $kT = 10$ eV, $\eta = 4$. Screening corrections to the reactivity, by a factor of the order of $\exp(\Gamma_e + \Gamma_i)$, are large; reactivity, however, becomes vanishingly small as temperature decreases, so that the net effect is still too minuscule to be of any practical interest in terms of reaction yield. In calculations, we have used the reactivity in the Gamow form, with the averaged astrophysical factor replaced by the zero-energy astrophysical factor, $S(0) = 2 \times 10^5$ keV barn [38].

Beam-driven scheme: It is well established that protons are the ions species preferentially accelerated in the laser-plasma interaction, basically because of the highest charge-to-mass ratio. In our irradiation conditions, protons are mostly accelerated in the forward direction [42]. A scheme based on the interaction of the forward proton stream with the shocked, warm target has proven to be effective in accounting for the measured fusion yield. For the sake of simplicity, we assume that the interaction takes place in a bulk which is homogeneous in density and temperature. Moreover, we suppose that the thermodynamic state of the bulk does not vary appreciably during the proton stream. We also assume that target ions have kinetic energies much lower than the proton ones, hence they are considered to be at rest in the reactions.

The overall number of α particles produced, N_α, is linked to the number of protons entering the target, N_p, by the obvious

relation

$$N_\alpha = 3 N_p P, \tag{6}$$

where P is the fusion probability (which in our case coincides with the thick-target yield). It is easy to show that

$$P = \eta \, n_{B,0} \, I(R), \tag{7}$$

where $n_{B,0}$ is the number density of ^{11}B nuclei at the mass density ρ_0 ($n_{B,0} = 4.16 \times 10^{22}$ cm^{-3}), I is an integral function of the proton path length x,

$$I(x) = \int_0^x \sigma[E(\xi)] \, d\xi, \tag{8}$$

and R is the total path length, which can be taken as the particle range to a good approximation. In Eq. (8), $E(x)$ is the proton energy during the slowing down in the bulk. We assume an initial energy $E(0) = E_0$ for all protons. The integral $I(R)$ can be evaluated more conveniently in the domain of energy, where it reads

$$I(E_0) = \int_0^{E_0} \sigma(E) \left(\frac{dE}{dx}\right)^{-1} dE, \tag{9}$$

where dE/dx is the proton stopping power (here taken as a positive quantity) and $E(R) = 0$ by definition. The analytic approximation of Nevins and Swain [2] has been used for $\sigma(E)$ in calculations [Fig. 1(a)]. It is worth noticing that because of Eq. (9), P depends on the mass stopping power, $\rho^{-1} dE/dx$. Otherwise stated, in the calculation of the fusion probability the mass stopping power accounts for the effects of both the density of reacting target nuclei and proton slowing down. Obviously, the mass stopping power is fully determined by the thermodynamic state (η, T) of the target.

Having measured N_α, we have actually calculated the fraction F of proton-to-laser energy needed to reproduce the experimental α yield:

$$F(E_0; \eta, T) \equiv \frac{N_p E_0}{E_L} = \frac{N_\alpha}{3 E_L} \frac{E_0}{P(E_0; \eta, T)}, \tag{10}$$

where we have used Eq. (6). The calculation of F has been performed for three possible scenarios of the thermodynamic state of the target bulk; results have then been benchmarked against the typical value of F in experiments at PALS ($F \simeq 0.05$ for $E_0 \gtrsim 700$ keV, corresponding to $N_p \gtrsim 2 \times 10^{14}$) [42] to assess which scenario is more plausible. The scenarios taken into consideration are the following:

1. Ordinary matter at density ρ_0

2. Fully degenerate plasma at $T = 0$, $4 < \eta < 7$

3. Maxwellian plasma at temperatures of the order of 1 keV, and $1 < \eta < 7$.

Plasma has been assumed to be fully ionized. As a term of reference, we have estimated—based on More's fitting [43]—that the fraction of electrons freed in BN by pressure ionization in the $T = 0$ limit is about 50% at $\eta = 4$, and overcomes 60% at $\eta = 7$. On another note, the Fermi energy of the degenerate free electron gas results in, e.g., 67 eV at $\eta = 4$, meaning that the degenerate scenario represents a good approximation for actual temperatures of the (highly)
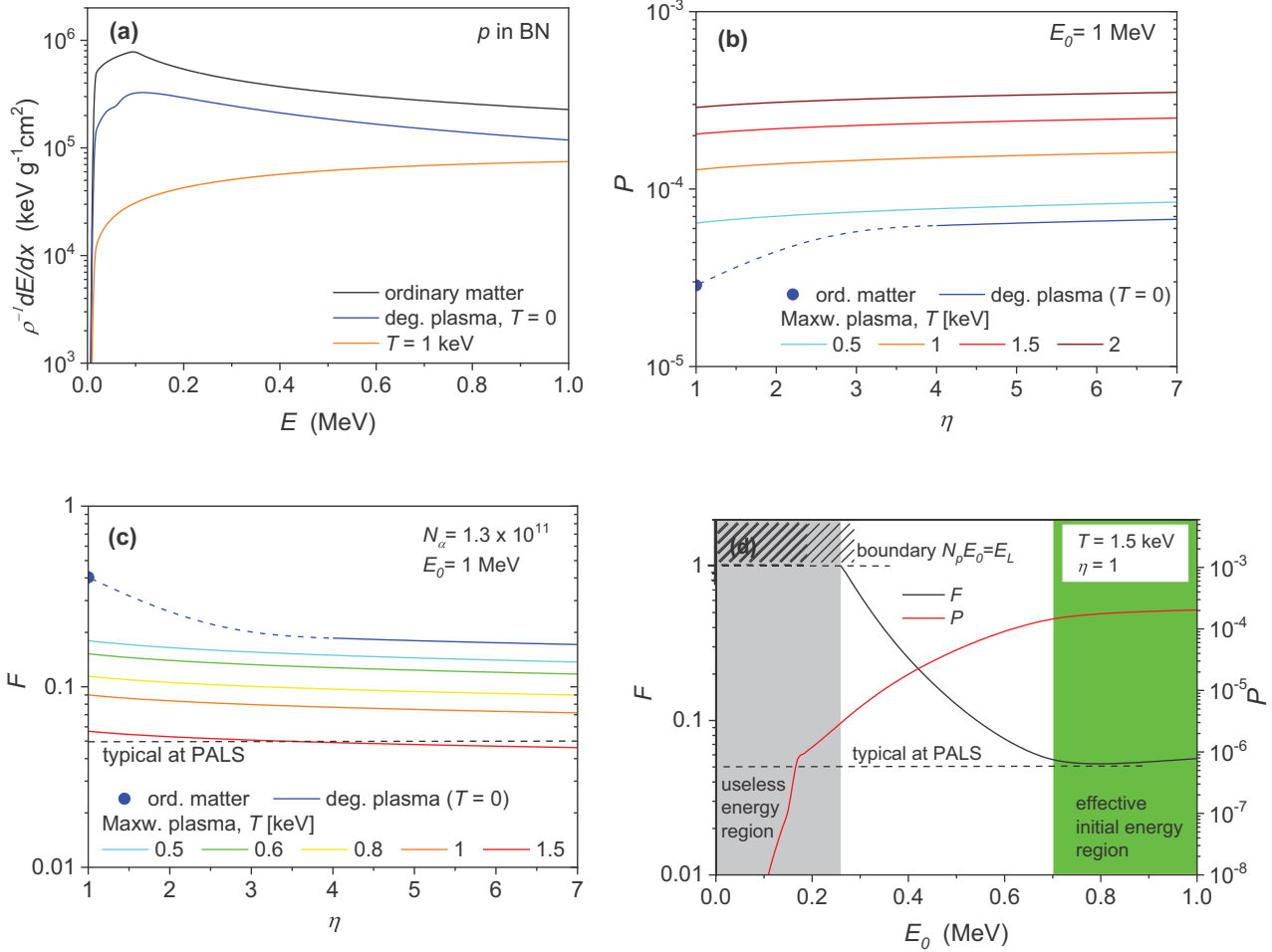
FIG. 7. (a) Electronic mass stopping power for protons in BN as a function of projectile energy, for ordinary bulk, fully degenerate plasma, and high-temperature plasma, respectively. Stopping powers are calculated at the density ρ_0. (b) Fusion probability for 1 MeV protons as a function of bulk compression, for values of interest of the temperature. The dashed curve represents intermediate ionization states between ordinary matter and degenerate plasma, and is drawn for eye guidance only. (c) Fraction of proton-to-laser energy needed to produce the given number of α particles, plotted as a function of bulk compression, for values of interest of the temperature. (d) Proton-to-laser energy fraction required for $N_\alpha = 1.3 \times 10^{11}$ as a function of the initial proton energy (black curve), in a bulk at $T = 1.5$ keV, $\eta = 1$. The relating fusion probability $P(E_0)$ is also shown (red curve).

compressed target which are much lower than 70 eV. On the contrary, target states with temperatures much higher than this value are well approximated by the Maxwellian plasma.

The stopping power in the case of degenerate plasma has been evaluated according to the formalism of Williams [44], in the free-electron-gas approximation. In the case of Maxwellian plasma, Sivukhin's slowing down model [45] has been used after Moreau [10]. Sivukhin's model represents a good compromise between accuracy and computational complexity in parametric studies (η and T are varied in our case), as long as the underlying Coulomb logarithm does not break down. For dE/dx in ordinary matter, data from SRIM tables [36] have been used, which are based on the Bethe-Bloch formula with corrections. In all cases, only the electronic stopping power has been considered, being the nuclear one negligible for our purposes. Example plots of the mass stopping power in BN are shown in Fig. 7(a) for the three different scenarios, as a function of proton energy. While the normalization over ρ renders the Bethe-Bloch stopping power independent of density (what makes $\rho^{-1}dE/dx$

a convenient quantity to deal with), in the case of both the degenerate and Maxwellian plasma, a residual dependency holds. The curves for these two cases have been calculated at the density ρ_0, for the sake of comparison with the curve for ordinary matter. The differences in magnitude are striking. While the curves for ordinary matter and degenerate plasma exhibit a similar shape, despite a difference in magnitude by a factor of approximately 2, the curve representative of high-temperature plasma shows a very different behavior, namely, a monotonous decrease as projectile energy lowers down. We recall that, as a general rule, at high density the mass stopping power decreases with increasing ionization and temperature of the medium.

Plots of P versus η are shown in Fig. 7(b) for the scenarios under investigation. Calculations refer to protons with $E_0 = 1$ MeV. We have neglected the collateral fusion reaction $^{10}\text{B}(p, \alpha)^7\text{Be}$, after verifying that in all cases it contributes to N_α less than 2%. As expected, P is enhanced by the temperature of the medium and reaches the order of 10^{-4} as T approaches 1 keV. Less obvious is its behavior against η: The

curves exhibit a monotonic increment with increasing compression, which indicates a slight advantage in inducing fusion inside a shocked target. The advantage is more significant at low temperature, moving from ordinary matter to degenerate plasma (blue curve). This feature is due to the tendency of the mass stopping power in plasmas to slightly decrease with increasing density.

Relevant plots of F versus η are shown in Fig. 7(c), with $N_\alpha = 1.3 \times 10^{11}$. One immediately notes that the value for ordinary matter ($F = 0.4$) is too high to be realistic. The curve corresponding to the fully degenerate cold plasma marks lower values ($F \simeq 0.2$), though still very little realistic. Expected values of F are being reproduced at bulk temperatures slightly exceeding 1 keV. We emphasize that the dependence of F on η is quite weak for a fully ionized plasma, whether degenerate or Maxwellian. The behavior of F tends, on the one hand, to limit the uncertainty on T, on the other hand, to increase that on η. Considering, e.g., $T = 1.5$ keV, $\eta = 1$ (on average throughout the proton interaction volume), F has been plotted as a function of E_0 in Fig. 7(d). The plot rules out any major contribution of low-energy protons (strictly speaking, below 250 keV) to the α yield; indeed, a so high number of such protons would be needed that their overall initial kinetic energy would exceed the energy of the laser pulse. This observation, in particular, rules out any role of the small fusion resonance at 160 keV. For the sake of completeness, a plot of P as a function of E_0 is also displayed in Fig. 7(d). It shows well how small fusion probability is and how quickly it drops at low proton energy. Another meaningful feature of the behavior of F against E_0 is that the curve is rather flat in the energy region ranging from about 0.7 to 1 MeV. As it is obvious from Eq. (10), if F keeps constant while varying E_0, then the number of available protons N_p has to scale as $1/E_0$, and P as E_0. The constancy of F implies that the assessment of the bulk temperature we have performed at $E_0 = 1$ MeV [Fig. 7(c)] is practically independent from the choice of a specific value of E_0, for $0.7 \lesssim E_0 \lesssim 1$ MeV. This makes our approximate method of inference, based on a single representative value of proton energy, more robust and realistic. We finally observe that having F its minimum value in the region of constancy, this region is also the most energetically efficient in the production of α particles (namely, in terms of number of fusion reactions per unit total proton energy).

Kinetic energy versus path length in the hot, shocked BN bulk at $T = 1.5$ keV has been plotted in Fig. 8 for protons with $E_0 = 1$ MeV. The path length is given in mass-thickness units since the underlying mass stopping power is very weakly dependent on density, as mentioned. One notes that the proton range approaches 4.2×10^{-2} g/cm^2 (as a term of comparison, the range of 1 MeV protons in ordinary BN is 0.30×10^{-2} g/cm^2 [36]). The bulk thickness needed to build the α yield up is much lower, though. The fusion probability build-up integral $I(\rho x)$ has also been plotted in the same graph, according to Eq. (8). It exhibits a wide plateau which advantageously limits the fusion-effective thickness, making it compatible with the energetics of the laser-target interaction, as discussed in the following. As a figure of merit, the proton path length corresponding to 90% of the asymptotic value of I is about 1.6×10^{-2} g/cm^2. This in turn corresponds to a cutoff proton energy for α production of about 400 keV (dashed-line
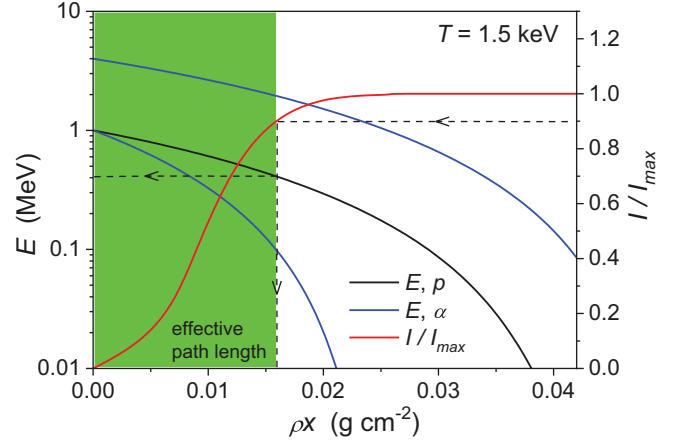
FIG. 8. Energy vs path-length curves for protons and α particles in a BN bulk at $T = 1.5$ keV. Initial energies are 1 MeV for protons; 1 MeV and 4 MeV for α particles, respectively. The normalized fusion probability up to a distance ρx, $I(\rho x)/I_{\max}$, is also shown during proton slowing down. Its wide plateau limits the thickness of the bulk region, which is needed for α production (dashed-line construction). Both groups of α particles have enough kinetic energy to leave that region.

construction). Moreover, the necessary bulk thickness is further reduced by the effect of multiple scattering, which lengthens the proton path compared to the penetration depth. By using the formulation of Lynch and Dahl [46], we estimate that in our case the penetration depth is about 15% shorter than the path length when $\rho x = 1.6 \times 10^{-2}$ g/cm^2. Consequently, we end up with a required bulk thickness of about 1.3×10^{-2} g/cm^2.

In the ideal-gas, steady-state approximation (i.e., neglecting shock dynamics, ionization work, and losses), the energy E_h needed to heat the bulk up to the temperature T is given by the left-hand side of Eq. (4) when $n_B = \eta n_{B,0}$ and $V = Sd$, where d is the effective bulk thickness and S is the area of the laser spot. Because thermal equilibrium between electrons and ions is not required in the beam-driven fusion scheme and is likely to not take place in the timescale of the processes under consideration, we can regard T as the electron temperature only and the ions as cold, neglecting their degrees of freedom. With $kT = 1.5$ keV, $\rho d = 1.3 \times 10^{-2}$ g/cm^2, $S = 5.03 \times 10^{-5}$ cm^2 (corresponding to a spot radius of 40 μm), we find $E_h \simeq 70$ J. This value is well below the energy absorbed in the interaction between the laser beam and the target, which is estimated [37] at a fraction of 30% of E_L in our irradiation conditions, i.e., 200 J. We present this as a mere argument of plausibility for our simple model, well aware of the large uncertainties affecting the experimental α yield, expected proton yield, stopping power models, and estimate of the bulk temperature.

Energy-path curves for α particles are also shown in Fig. 8, for initial energies of 1 and 4 MeV. In both cases, α particles are able to escape the effective bulk region while propagating backward towards the detectors. However, from this crude two-group approximation of the α spectrum, it is evident that only the 4 MeV particles produced sufficiently close to the target surface (actually, the ablation front) would have enough energy to pass through the filters on CR39 detectors (3 MeV

cutoff). This implies that if the α particles emitted backward were not accelerated, we would measure considerably lower yields.

To conclude, we also observe that any contribution to α particle generation coming from the backward-accelerated protons is negligible, because of their much lower yield compared to the forward stream [42] and the lower mass thickness of the plume compared to the compressed target bulk. In addition, at target (or plume) densities and temperatures accessible in our experiment, we rule out, on the basis of the latest findings [47], any possible contribution coming from avalanche fusion reactions sustained by collisional energy transfer from α particles to protons [48].

B. α-particle energy distribution

We have reported experimental evidence of a shift towards higher energies in the α spectra, which were measured in the backward direction. Such a shift is too large to be ascribed to the initial proton energy; it rather seems compatible with the increase in kinetic energy, zeV, induced on a particle of charge ze by an external electrostatic potential V, when $z = 2$ and $V \simeq 1.5$ MV, which resembles the laser-driven potential accelerating protons backward. Evidence of unexpectedly high α energies can also be found in the works of Belyaev *et al.* [20] and Picciotto *et al.* [23], who used a laser-target interaction scheme similar to that adopted in this work and revealed α particles generated on the target or in its proximity and propagating backward. In particular, Belyaev *et al.* [20], who worked at a laser intensity of the order of 10^{18} W/cm^2, reports α energies up to 10 MeV and attributes such a high value to the reaction kinematics of protons with comparable energy (though not measured).

On the contrary, Labaune *et al.* [22,49], who worked at an even higher laser intensity (6×10^{18} W/cm^2) and comparable pulse energy (of the order of 10 J), does not report increased energies in the α spectra, in spite of proton energies up to about 6 MeV. In this experiment, however, the colliding protons and boron ions originated from two different targets; in particular, the laser-accelerated proton beam interacted with a secondary boron target, in the form of a solid or plasma, "far" from its target of origin. This observation would suggest that the energy augmentation of the α particles appears when those are produced close enough to the target emitting protons to be coaccelerated with them. We put forward that this effect, rather than fusion reaction kinematics, might have been responsible for the high α energies measured by Belyaev *et al.* [20] and Picciotto *et al.* [23].

In conclusion, we claim an evidence for laser acceleration of fusion α particles as well. Such an effect increases the reaction energy yield well beyond the Q value, thus improving—in principle—the laser-to-fusion energy conversion efficiency. The effect might play a major role in possible applications of pB fusion such as laser-driven space propulsion. Concerning this latter, in particular, the directionality of the accelerating electric field would further contribute to increase the momentum of the propulsion jet.

C. Perspectives

Since 2005, when Belyaev *et al.* [20] published the first experimental results about the laser-driven pB reaction using
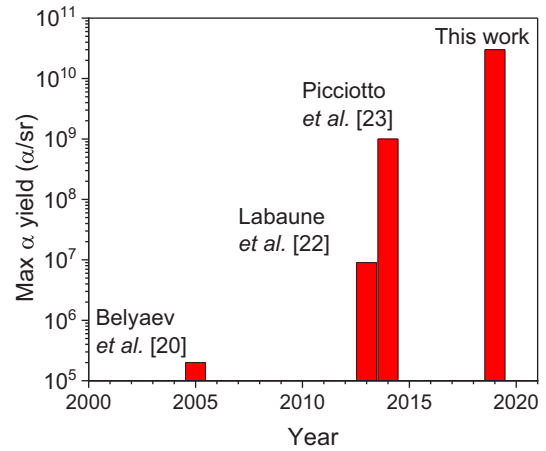
FIG. 9. Progression of the most important experimental achievements reported in the literature in terms of maximum α particles/sr.

a borated target, the progression of the α-particle yield has raised steeply. Figure 9 shows the most important experimental achievements reported in literature in terms of particles/sr. The α yield has increased by a factor of 10^5 in less than 15 years of sparse experiments. It has to be noted that these results are not part of a coordinated research program but stem from basic trials to test the effects of specific laser characteristics or target configurations. Nevertheless, not only the progression of the α yield is encouraging for further developments, but we find somewhat surprising the relative ease of inducing and measuring the pB fusion reaction in laser-driven schemes.

Concerning our experiment, in particular, laser and target characteristics are far from being the ideal ones in the quest for ignition [13]. Among other things, we use a target which is not hydrogen-rich as well as not isotopically enriched in ^{11}B. Taking also into account that we have adopted a conservative estimate of the α yield, we feel confident that with a pure boron target enriched in the isotope 11 and improved yield of accelerated protons (by, e.g., heavy H doping), the order of 10^{12} α particles is at easy reach at PALS.

Such a surprising figure is due to the fact that in our experiment, fusion is induced by protons with energies far outside the (local) thermal equilibrium of the target, which is made possible by the mechanism of laser acceleration (indeed, the thermonuclear yield is absolutely negligible in our scheme, as we have shown). At laser intensities much higher than that used in this work, above 10^{18} W/cm^2, the acceleration mechanism might be dramatically enhanced by the ponderomotive force, ultimately resulting in the *volume* acceleration of ions in a solid target, as predicted in Ref. [12]. In solid-density H^{11}B fuel (hypothetical material), the proton current—which could exceed 10^{10} A/cm^2 [50]—and the α-particle flux from beam-driven reactions could deposit enough heat to trigger a thermonuclear reaction wave; under lateral confinement by a strong magnetic field, the fusion flame could burn long enough to yield a net gain [12,13].

Laser systems capable to irradiate at 10^{20} to 10^{21} W/cm^2 as well as laser-driven techniques for the induction of kTesla magnetic fields [51,52] are becoming available. For instance, a

10 PW (1.5 kJ, 150 fs) laser (denominated L4) is envisaged to become operational at the ELI facility [53], Czech Republic, by the end of 2020. Relying on technological capabilities of this kind, our latest findings and the recent theoretical predictions urgently call for a dedicated research program to pursue ignition of $H^{11}B$ fuel and explore further potentialities of laser-driven pB fusion.

V. CONCLUSIONS

The possibility of enhancing the yield of α particles produced by laser-driven proton-boron nuclear fusion has been studied in this paper. Using boron-nitride-thick targets interacting with a laser beam at the intensity of 3×10^{16} W/cm^2, we have reached a total number of α particles of about 1.3×10^{11}, a value never measured in previous works.

We have shown that the production of α particles is not of thermonuclear nature. The huge yield measured is rather explicable in terms of a beam-driven fusion scheme, based on the interaction of the laser-driven proton stream in the forward direction with ^{11}B nuclei residing in the target.

Furthermore, we have found experimental evidence of a shift towards higher energies in the α spectra, which were measured in the backward direction. This shift is probably due to the laser-driven potential accelerating protons backward, which provides the α particles with an extra kinetic energy of the order of $2e \times V = 3$ MeV, with $V \simeq 1.5$ MV. This effect might also have manifested, though unrecognized, in previous experiments using a setup similar to this work [20,23].

Our findings pave the way to a dedicated research programme in view of assessing the viability of laser-driven pB fusion as a potential source of energy with enormously reduced environmental impact due to the neutron-free character of the reaction.

[1] M. L. E. Oliphant and E. Rutherford, Experiments on the transmutation of elements by protons, Proc. R. Soc. A **141**, 259 (1933).

[2] W. M. Nevins and R. Swain, The thermonuclear fusion rate coefficient for p–11B reactions, Nucl. Fusion **40**, 865 (2000).

[3] J. Quebert and L. Marquez, Effets des résonances de 12C sur l'émission de particules alpha dans la réaction 11B(p, 3α), Nucl. Phys. A **126**, 646 (1969).

[4] S. Stave, M. W. Ahmed, R. H. France III, S. S. Henshaw, B. Müller, B. A. Perdue, R. M. Prior, M. C. Spraker, and H. R. Weller, Understanding the 11B(p,α)$\alpha\alpha$ reaction at the 0.675 MeV resonance, Phys. Lett. B **696**, 26 (2011).

[5] V. F. Dimitriev, α-particle spectrum in the reaction p + 11B $\rightarrow$ α + 8Be* $\rightarrow$ 3α, Phys. At. Nucl. **72**, 1165 (2009).

[6] H. W. Becker, C. Rolfs, and H. P. Trautvetter, Low-energy cross sections for11B(p, 3α), Z. Phys. A: Atomic Nuclei **327**, 341 (1987).

[7] J. Liu, X. Lu, X. Wang, and W. K. Chu, Cross-sections of 11B(p, α) ^{8}Be reaction for boron analysis, Nucl. Instrum. Methods Phys. Res. B **190**, 107 (2002).

[8] M. C. Spraker, M. W. Ahmed, M. A. Blackston, N. Brown, R. H. France III, S. S. Henshaw, B. A. Perdue, R. M. Prior, P.-N. Seo, S. Stave, and H. R. Weller, The 11B(p, α)8Be $\rightarrow$ α + α and the 11B(α, α)11B reactions at energies below 5.4 MeV, J. Fusion Energ. **31**, 357 (2012).

[9] M. H. Sikora and H. R. A. Weller, New evaluation of the ^{11}B(p, α)$\alpha\alpha$ reaction rates, J. Fusion Energy **35**, 538 (2016).

[10] D. C. Moreau, Potentiality of the proton-boron fuel for controlled thermonuclear fusion, Nucl. Fusion, **17**, 13 (1977).

[11] N. Rostoker, A. Qerushi, and M. Binderbauer, Colliding beam fusion reactors, J. Fusion Energy **22**, 83 (2004).

[12] H. Hora, G. Korn, L. Giuffrida, D. Margarone, A. Piciotto, J. Krasa, K. Jungwirth, J. Ullschmied, P. Lalousis, S. Eliezer, G. H. Miley, S. Moustaizis, and G. Mourou, Fusion energy using avalanche increased boron reactions for block-ignition by ultrahigh power picosecond laser pulses, Laser Part. Beams **33**, 607 (2015).

[13] H. Hora, S. Eliezer, G. J. Kirchhoff, N. Nissim, J. X. Wang, P. Lalousis, Y. X. Xu, G. H. Miley, J. M. Martinez-Val, W. McKenzie, and J. Kirchhoff, Road map to clean energy using laser beam ignition of boron-hydrogen fusion, Laser Part. Beams **35**, 730 (2017).

[14] C. Ohlandt, T. Kammash, and K. G. Powell, A design study of a p-11B gasdynamic mirror fusion propulsion system, AIP Conf. Proc. **654**, 490 (2003).

[15] D.-K. Yoon, J.-Y. Jung, and T. S. Suh, Application of proton boron fusion reaction to radiation therapy: A Monte Carlo simulation study, Appl. Phys. Lett. **105**, 223507 (2014).

[16] L. Giuffrida, D. Margarone, G. A. P. Cirrone, A. Picciotto, G. Cuttone, and G. Korn, Prompt gamma ray diagnostics and enhanced hadron-therapy using neutron-free nuclear reactions, AIP Adv. **6**, 105204 (2016).

[17] G. A. P. Cirrone, L. Manti, D. Margarone, G. Petringa, L. Giuffrida, A. Minopoli, A. Picciotto, G. Russo, F. Cammarata, P. Pisciotta *et al.*, First experimental proof of Proton Boron Capture Therapy (PBCT) to enhance protontherapy effectiveness, Sci. Rep. **8**, 1141 (2018).

[18] G. Petringa, G. A. P. Cirrone, C. Caliri, G. Cuttone, L. Giuffrida, G. La Rosa, R. Manna, L. Manti, V. Marchese, C. Marchetta *et al.*, Prompt gamma-ray emission for future imaging applications in proton-boron fusion therapy, J. Instrum. **12**, C03059 (2017).

[19] G. Petringa, G. A. P. Cirrone, C. Caliri, G. Cuttone, L. Giuffrida, G. La Rosa, R. Manna, L. Manti, V. Marchese, C. Marchetta

et al., Study of gamma-ray emission by proton beam interaction with injected boron atoms for future medical imaging applications, J. Instrum. **12**, C03049 (2017).

[20] V. S. Belyaev, A. P. Matafonov, V. I. Vinogradov, V. P. Krainov, V. S. Lisitsa, A. S. Roussetski, G. N. Ignatyev, and V. P. Andrianov, Observation of neutronless fusion reactions in picosecond laser plasmas, Phys. Rev. E **72**, 026406 (2005).

[21] S. Kimura, A. Anzalone, and A. Bonasera, Comment on "Observation of neutronless fusion reactions in picosecond laser plasmas," Phys. Rev. E **79**, 038401 (2009).

[22] C. Labaune, C. Baccou, S. Depierreux, C. Goyon, G. Loisel, V. Yahia, and J. Rafelski, Fusion reactions initiated by laser-accelerated particle beams in a laser-produced plasma, Nat. Commun. **4**, 2506 (2013).

[23] A. Picciotto, D. Margarone, A. Velyhan, P. Bellutti, J. Krasa, A. Szydlowsky, G. Bertuccio, Y. Shi, A. Mangione, J. Prokupek *et al.*, Boron-Proton Nuclear-Fusion Enhancement Induced in Boron-Doped Silicon Targets By Low-Contrast Pulsed Laser, Phys. Rev. X **4**, 031030 (2014).

[24] D Margarone, A. Picciotto, A. Velyhan, J. Krasa, M. Kucharik, A. Mangione, A. Szydlowsky, A. Malinowska, G. Bertuccio, Y. Shi *et al.*, Advanced scheme for high-yield laser driven nuclear reactions, Plasma Phys. Control. Fusion **57**, 014030 (2015).

[25] K. Jungwirth, A. Cejnarova, L. Juha, B. Kralikova, J. Krasa, E. Krousky, P. Krupickova, L. Laska, K. Masek, T. Mocek *et al.*, The prague asterix laser system, Phys. Plasmas **8**, 2495 (2001).

[26] S. Rudolph, Boron nitride (BN), Am. Ceram. Soc. Bull. **79**, 50Q (2000).

[27] J. Krása, D. Klír, K. Rezác, J. Cikhardt, M. Krůs, A. Velyhan, M. Pfeifer, S. Buryšková, J. Dostál, T. Burian *et al.*, Production of relativistic electrons, MeV deuterons and protons by sub-nanosecond terawatt laser, Phys. Plasmas **25**, 113112 (2018).

[28] G. Bertuccio, D. Puglisi, L. Torrisi, and C. Lanzieri, Silicon carbide detector for laser-generated plasma radiation, Appl. Surf. Sci. **272**, 128 (2013).

[29] D. Margarone, J. Krasa, L. Giuffrida, A. Picciotto, L. Torrisi, T. Nowak, P. Musumeci, A. Velyhan, J. Prokupek, L. Laska *et al.*, Full characterization of laser-accelerated ion beams using Faraday cup, silicon carbide, and single-crystal diamond detectors, J. Appl. Phys. **109**, 103302 (2011).

[30] G. Milluzzo, V. Scuderi, A. Alejo, A. G. Amico, N. Booth, M. Borghesi, G. A. P. Cirrone, G. Cuttone, D. Doria, J. Green *et al.*, A new energy spectrum reconstruction method for Time-Of-Flight diagnostics of high-energy laser-driven protons, Rev. Sci. Inst. **90**, 083303 (2019).

[31] V. Scuderi, A. Amato, A. G. Amico, M. Borghesi, G. A. Pablo Cirrone, G. Cuttone, A. Fajstavr, L. Giuffrida, F. Grepl, G. Korn *et al.*, Diagnostics and dosimetry solutions for multidisciplinary applications at the ELIMAIA beamline, Appl. Sci. **8**, 1415 (2018).

[32] T. W. Jeong, P. K. Singh, C. Scullion, H. Ahmed, P. Hadjisolomou, C. Jeon, H. Yun, K. F. Kakolee, M. Borghesi, and S. Ter-Avetisyan, CR-39 track detector for multi-MeV ion spectroscopy, Sci. Rep. **7**, 2152 (2017).

[33] J. Krasa, L. Laska, K. Rohlena, M. Pfeifer, J. Skala, B. Kralikova, P. Straka, E. Woryna, and J. Wolowski, The effect of laser-produced plasma expansion on the ion population, Appl. Phys. Lett. **75**, 2539 (1999).

[34] D. Margarone, J. Krasa, A. Picciotto, L. Torrisi, L. Laska, A. Velyhan, J. Prokupek, L. Ryc, P. Parys, J. Ullschmied *et al.*, High current, high energy proton beams accelerated by a sub-nanosecond laser, Nucl. Instrum. Methods Phys. Res. A **653**, 159 (2011).

[35] D. Margarone, J. Krasa, L. Laska, A. Velyhan, T. Mocek, J. Prokupek, E. Krousky, M. Pfeifer, S. Gammino, L. Torrisi, J. Ullschmied, and B. Rus, Measurements of the highest acceleration gradient for ions produced with a long laser pulse, Rev. Sci. Instrum. **81**, 02A506 (2010).

[36] J. F. Ziegler and J. P. Biersack, SRIM-2013, http://www.srim.org (2013).

[37] S. Yu. Gus'kov, N. N. Demchenko, A. Kasperczuk, T. Pisarczyk, Z. Kalinowska, T. Chodukowski, O. Renner, M. Smid, E. Krousky, M. Pfeifer *et al.*, Laser-driven ablation through fast electrons in PALS-experiment at the laser radiation intensity of 1–50 PW/cm^2, Laser Part. Beams **32**, 177 (2014).

[38] J. C. Pain, Equation-of-state model for shock compression of hot dense matter, Phys. Lett. A **362**, 120 (2007).

[39] R. Liska, M. Kuchřík, J. Limpouch, O. Renner, P. Váchal, L. Bednárik, and J. Velechovský, ALE method for simulations of laser-produced plasmas, in *Finite Volumes for Complex Applications VI Problems & Perspectives*, edited by J. Fořt, J. Fürst, J. Halama, R. Herbin, and F. Hubert, Springer Proceedings in Mathematics, Vol. 4 (Springer, Berlin, Heidelberg, 2011), pp. 857–873.

[40] J. Krasa, K. Jungwirth, E. Krousky, L. Laska, K. Rohlena, M. Pfeifer, J. Ullschmied, and A. Velyhan, Temperature and centre-of-mass energy of ions emitted by laser-produced polyethylene plasma, Plasma Phys. Control. Fusion **49**, 1649 (2007).

[41] S. Atzeni and J. Meyer-ter-Vehn, *The Physics of Inertial Fusion* (Oxford University Press, Oxford, 2004).

[42] D. Margarone, A. Velyhan, J. Dostal, J. Ullschmied, J. P. Perin, D. Chatain, S. Garcia, P. Bonnay, T. Pisarczyk, R. Dudzak *et al.*, Proton Acceleration Driven by a Nanosecond Laser from a Cryogenic thin Solid-Hydrogen Ribbon, Phys. Rev. X **6**, 041030 (2016).

[43] R. M. More, Atomic physics in dense plasmas, in *Nuclear Fusion by Inertial Confinement*, edited by G. Velarde, Y. Ronen, and J. M. Martinez Val (CRC Press, Boca Raton, FL, 1993), pp. 151–184.

[44] M. M. R. Williams, The range of charged particles in a degenerate electron gas (applied to fusion reactors), J. Phys. D **8**, 2138 (1975).

[45] D. V. Sivukhin, Coulomb collisions in a fully ionized plasma, in *Reviews of Plasma Physics*, edited by M. A. Leontovich (Consultants Bureau, New York, 1966), Vol. 4, p. 93.

[46] G. R. Lynch and O. I. Dahl, Approximations to multiple Coulomb scattering, Nucl. Instr. Meth. B **58**, 6 (1991).

[47] F. Belloni, D. Margarone, A. Picciotto, F. Schillaci, and L. Giuffrida, On the enhancement of p-^{11}B fusion reaction rate in laser-driven plasma by $\alpha \rightarrow$ p collisional energy transfer, Phys. Plasmas **25**, 020701 (2018).

[48] S. Eliezer, H. Hora, G. Korn, N. Nissim, and J. M. Martinez Val, Avalanche proton-boron fusion based on elastic nuclear collisions, Phys. Plasmas **23**, 050704 (2016).

[49] C. Labaune, C. Baccou, V. Yahia, C. Neuville, and J. Rafelski, Laser-initiated primary and secondary nuclear reactions in boron-nitride, Sci. Rep. **6**, 21202 (2016).

[50] H. Hora, G. H. Miley, M. Ghoranneviss, B. Malekynia, N. Azizic, and X.-T. He, Fusion energy without radioactivity: Laser ignition of solid hydrogen–boron (11) fuel, Energy Environ. Sci. **3**, 479 (2010).

[51] J. J. Santos, M. Bailly-Grandvaux, L. Giuffrida, P. Forestier-Colleoni, S. Fujioka, Z. Zhang, P. Korneev, R. Bouillaud, S.

Dorard, D. Batani *et al.*, Laser-driven platform for generation and characterization of strong quasi-static magnetic fields, New J. Phys. **17**, 083051 (2015).

[52] F. Schillaci, M. De Marco, L. Giuffrida, S. Fujioka, Z. Zhang, G. Korn, and D. Margarone, Numerical simulations to model laser-driven coil-capacitor targets for generation of kilo-Tesla magnetic fields, AIP Adv. **8**, 025103 (2018).

[53] https://www.eli-beams.eu/.